Synthesis of Platinum Dendrites and Nanowires Via Directed Electrochemical Nanowire Assembly

ARTICLE *in* NANO LETTERS · FEBRUARY 2011

Impact Factor: 13.59 · DOI: 10.1021/nl1039956 · Source: PubMed

NANO LETTERS

LETTER

pubs.acs.org/NanoLett

Synthesis of Platinum Dendrites and Nanowires Via Directed Electrochemical Nanowire Assembly

Jason K. Kawasaki† and Craig B. Arnold*

Department of Mechanical and Aerospace Engineering and Princeton Institute for the Science and Technology of Materials (PRISM), Princeton University, Princeton, New Jersey 08544, United States

ABSTRACT: Directed electrochemical nanowire assembly is a promising high growth rate technique for synthesizing electrically connected nanowires and dendrites at desired locations. Here we demonstrate the directed growth and morphological control of edge-supported platinum nanostructures by applying an alternating electric field across a chloroplatinic acid solution. The dendrite structure is characterized with respect to the driving frequency, amplitude, offset, and salt concentration and is well-explained by classical models. Control over the tip diameter, side branch spacing, and amplitude is demonstrated, opening the door to novel device architectures for sensing and catalytic applications.

KEYWORDS: Platinum nanowire, platinum dendrite growth, DENA, electrochemical deposition, metal nanodendrite, nanowire sensor

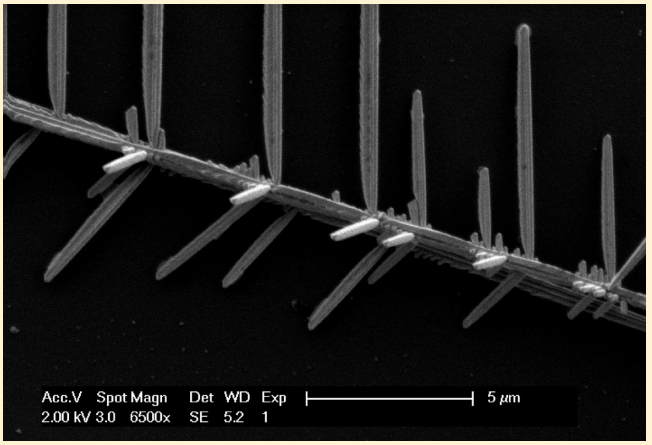

Metallic nanowires are an important class of materials for the study of low-dimensional transport phenomena and growth of such structures in a directed manner enables their use as a building block for electronic, optoelectronic, and NEMS devices.[1,2] Currently a number of techniques exist for the synthesis of both randomly oriented and mounted arrays of metallic nanowires, including electrospinning[3] and template driven electrodeposition[4,5] respectively; however, for certain applications, secondary processing steps such as electrostatic trapping,[6] optical trapping,[7] dielectrophoresis,[8,9] or microfluidic flow[10] are required to orient and place single nanowires at desired locations. In contrast, directed growth techniques such as directed gas phase growth via chemical vapor deposition[11] or electrochemical deposition in prepatterned structures[12] can be used to grow and place single crystal metallic nanowires between microelectrodes in a single step. However such techniques can be very slow, less than one micrometer per minute, limiting their utility in applications where high aspect ratio features are required.

Metallic dendrites are another important class of materials that are attractive due to their high surface-area-to-volume ratio and their high degree of connectivity. These properties make dendrites useful for a number of applications including catalysis,[13,14] chemical sensing,[15,16] and surface enhanced Raman scattering.[16] However, the resulting dendrites are typically dispersed in solution,[14,16,17] and thus just as for nanowires, secondary processing steps would be required to orient and place them at the desired locations.

Directed electrochemical nanowire assembly (DENA) is a promising one-step, high growth rate approach to producing oriented, single crystal nanowires and dendrites. In this method, an alternating electric field applied to a salt solution induces the crystallization of metallic wires or dendrites. The direction of these structures is guided by the electric field[18] and the resulting nanowires grow at specified locations and orientations as defined by the electrode configuration. In contrast to gas phase growth, this solution-based method can achieve much faster growth rates, on the order of tens of micrometers per second, and since growth is achieved at atmosphere it is relatively inexpensive and easy to use. Furthermore, it is achieved at room temperature, which is in contrast to the elevated substrate temperatures required in methods such as MBE and MOCVD. DENA was first demonstrated by Cheng et al.,[19] who showed that 75 nm diameter palladium nanowires could be grown at prescribed locations from a palladium acetate solution. Growth has also been demonstrated for indium[20] and gold.[21]

This letter explores the use of DENA to grow Pt dendrites and nanowires for sensor and catalysis development. Pt is chosen primarily for its chemical inertness, catalytic performance, and thermoelectric properties. We explore the conditions that control growth directionality and dendrite morphology including driving frequency, amplitude, offset, and salt additives. The main stem diameter is dependent on driving frequency, whereas the side branch spacing and magnitude are primarily controlled by voltage amplitude and salt concentration. The experimental results are explained in the context of classical dendrite growth models. The growth of nanostructures ranging from treelike, multibranched dendrites to single, nonbranching, high aspect ratio nanowires between two microelectrodes is demonstrated.

Received: November 14, 2010
Revised: December 21, 2010

dx.doi.org/10.1021/nl1039956 | *Nano Lett.* XXXX, XXX, 000–000

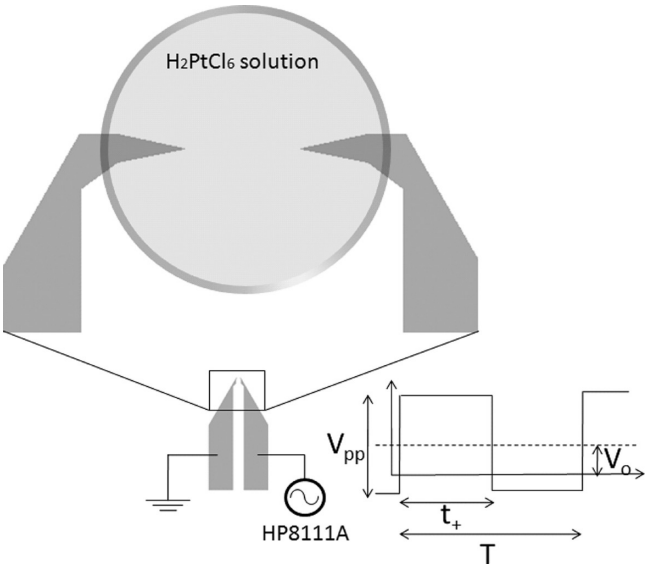

Figure 1. DENA experimental setup.

Figure 1 shows the wire growth apparatus. The electrodes are patterned via photolithography and consist of a 100 nm thick Pt top layer, 10 nm thick Ti adhesion layer, and 500 nm SiO_2 insulating layer on an silicon substrate. The gap between the electrodes is 60 μm. A 1 μL droplet of 24 mM aqueous chloroplatinic acid solution (H_2PtCl_6, Cole-Parmer) is placed across the electrodes, and a waveform generator (HP 8111A) is used to apply a square wave potential $V(t)$ across the gap. This potential drives the reduction of Pt cations from solution, resulting in Pt dendrites that grow from one electrode tip toward the other.

Growth is achieved by programming the desired frequency and then ramping to the desired voltage with the waveform generator. We examine growth for applied square waves in the range of frequencies 0−10 MHz and voltage magnitudes 0−30 V_{pp} (peak to peak). We also study the effects of adding a dc voltage offset (V_0, Figure 1), varying the duty cycle (defined as t_+/T, Figure 1), and adding NaCl to the electroplating solution. All growth is observed in situ under an optical microscope (Zeiss), and after growth, samples are rinsed in DI water and characterized via scanning electron microscope (Phillips XL30).

Since such large voltage magnitudes are used, a number of reaction pathways exist for the reduction of Pt. One such pathway is shown in eq 1 in which the hexachloroplatinate ion is directly reduced to elemental Pt, but other pathways may include the formation of intermediates, such as tetrachloroplatinate.

$$2H_3O^+ + PtCl_6^{2-} + 6H_2O \overset{V(t)}{\rightleftharpoons} Pt(s) + 6H_3O^+ + 6Cl^- + O_2(g) \quad (1)$$

We find that there are two primary growth regimes, planar electroplating and anisotropic dendrite growth. Below a minimum voltage magnitude ($V_{min} \approx 12V_{pp}$) and a minimum frequency ($\omega_{min} \approx 10$ kHz), the reduction results in planar electroplating on the electrode surface. Above these thresholds, highly branched dendrites form, as shown in Figure 2. These structures show classical dendrite behavior with sidebranches that point in crystallographic directions, a regular spacing between sidebranches, and a regular angle of 71° between stem and branch. The branching angle of 71° corresponds to the angle

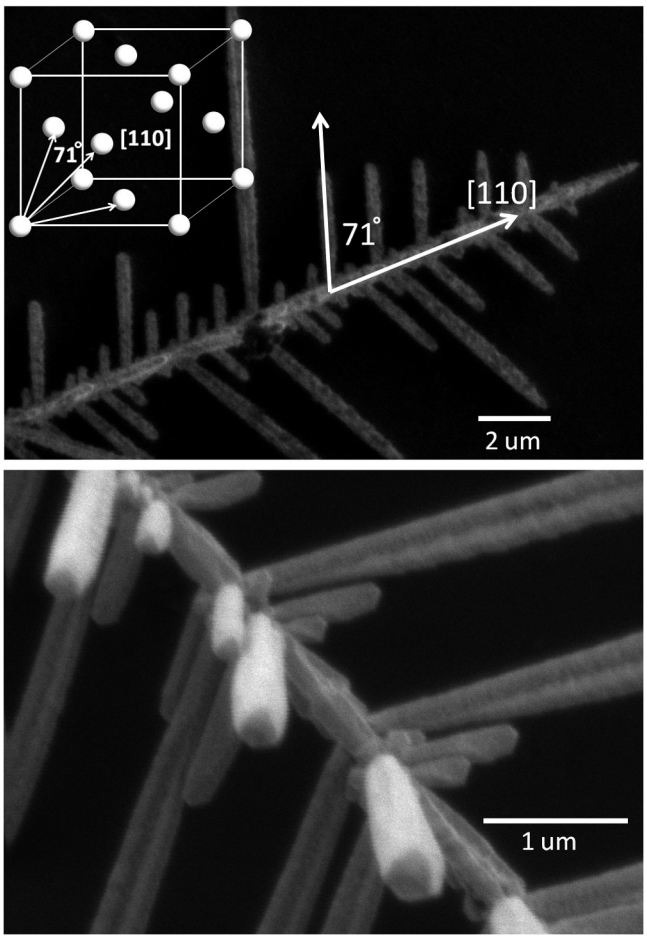

Figure 2. Dendrite grown via the DENA method at 2 MHz, 17.6 V_{pp}, V_0 = 0, 50% duty cycle. (top) SEM micrograph of the dendrite tip. The sidebranch angle of 71° likely corresponds to growth in the ⟨110⟩ directions of the fcc lattice. (bottom) Higher-resolution micrograph of the dendrite junction structure.

between the ⟨110⟩ close-packed directions directions of the face-centered cubic (fcc) lattice, suggesting that the Pt dendrites are single crystal and grow in the ⟨110⟩ (Figure 2a). These results are consistent with TEM studies of single crystal Pt nanoparticles, which have shown that the ⟨110⟩ are preferred growth directions while the {100} and {111} are preferred facets.[22]

The results also appear consistent with the picture for classical dendrite growth. In classic dendritic solidification, growth is driven by a thermal undercooling $\Delta = T_{melt} - T$.[23,24] At low absolute values of Δ, the solidification front is planar and stable. However as Δ increases, solidification becomes so rapid that temperature and concentration gradients build up at the solidification front. Here solidification becomes limited by the diffusion of latent heat away from the solidification front, and the result is the anisotropic propagation of instabilities (sidebranches). Additionally, a large Δ is also expected to increase the tip velocity v_{tip} and decrease the tip diameter ρ. Similar results are obtained for the electrolytic growth of dendrites, where instead of the undercooling, growth is driven by the overpotential η.[25]

Like electrolytic growth, in DENA the driving force is electrochemical. Here the oscillating potential $V(t)$, or the resulting electric field $E(t)$, drives the reduction of Pt cations from solution, leading to nucleation at the electrode tips and

dx.doi.org/10.1021/nl1039956 |Nano Lett. XXXX, XXX, 000–000

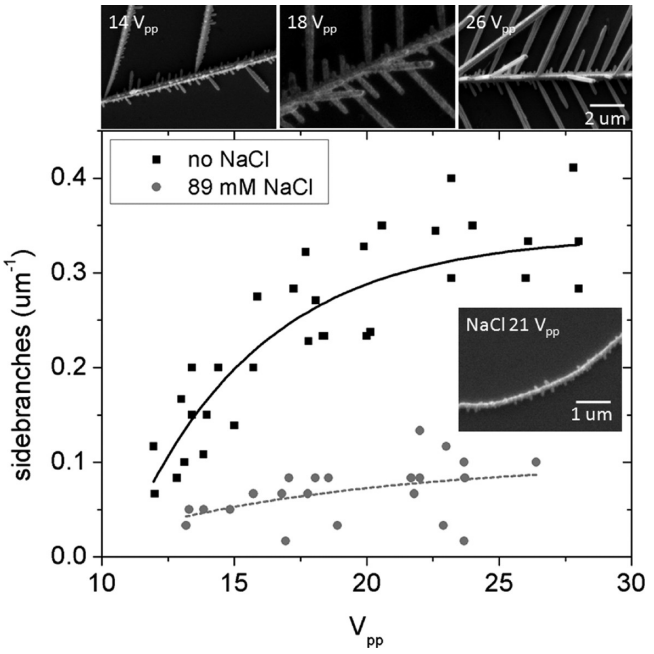

Figure 3. Plots of the side branching (number of branches per micrometer) versus voltage magnitude for chloroplatinic acid solutions without NaCl (squares, three SEM insets at top), and solutions with 89 mM NaCl (circles, SEM inset at right middle).

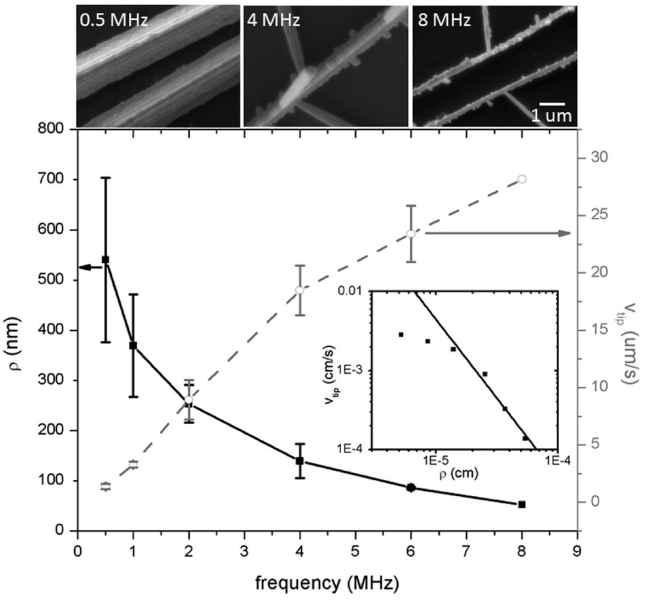

Figure 4. Plot of the tip velocity v_{tip} and diameter versus the frequency ω with accompanying scanning electron micrographs. Inset: Log−log plot of the tip velocity versus the radius. The straight line corresponds to a slope of −2, as predicted by eq 2.

crystallization of Pt dendrites. Side branch formation is caused by a similar instability as in the case of thermal dendrites. A large driving force leads to a reduced interface stability and thus a greater degree of side branching. However, note that whereas the classical dendrite growth examples had dc driving forces,[23−25] the driving force in DENA is ac. Hence the DENA driving force may be described by two components, the magnitude of the applied potential V_{pp} and its frequency ω.

We first examine the effects of V_{pp}. Previous studies have shown that a large applied V_{pp} leads to a greater degree of side branching in Au and In systems,[18,20,21] and we demonstrate a similar trend for Pt DENA growth. We find that the number of side branches per micrometer along the Pt main stem grows with increasing V_{pp} and these results are denoted by the black squares in Figure 3. A side branch is defined as any growth along the main stem that is of length greater than twice the diameter of the main stem. We also note that changing V_{pp} does not affect the tip velocity or tip radius. This observation lies in contrast with the expected behavior for classical dendritic solidification, in which the sidebranching, v_{tip}, and ρ are all expected to be controlled by the magnitude of the driving force.

As the V_{pp} decreases, there is an expected reduction in the degree of side branching, but it is not possible to reduce this to zero due to the planar electroplating regime that occurs at lower voltages. A minimum of approximately $V_{min} = 12\ V_{pp}$ is required to induce anisotropic dendrite growth, but as shown in Figure 3, this value still yields a considerable degree of side branching. Thus additional methods of suppression are needed to obtain nonbranching structures.

Addressing this demand, we find that the addition of NaCl to the electroplating solution results in a dramatic suppression of side branch formation. The presence of NaCl causes a shift to less branching as denoted by the gray circles in Figure 3. We identify two possible mechanisms leading to this side branch suppression. For one, the chlorine passivates the surface of the growing dendrite, for it is known that chlorine adsorbs readily on Pt.[26] Second, the Cl^- slows the reduction of Pt, as Cl^- is found on the right-hand side of eq 1. These two effects serve as a mechanism to stabilize the growing dendrite surface and inhibit side branch formation.

In addition to the magnitude of the driving force and the presence of salt, we also examine the effect of the ac frequency ω. We find that increasing the frequency increases the growth velocity v_{tip} and decreases the wire radius ρ (Figure 4) without affecting the degree of sidebranching. At frequencies greater than 5 MHz, the growth rate is in excess of 20 μm per second with nanowire radii reaching as small as 50 nm.

The observation that the growth velocity and radius of the wires are anticorrelated is consistent with classical dendritic solidification theory from which a stability analysis predicts that the tip velocity and tip radius of curvature ρ' are related by

$$v_{tip} = \frac{2d_0D}{\sigma}\frac{1}{\rho'^2} \qquad (2)$$

where D is the diffusion coefficient, d_0 is the capillary length, and σ is the stability criterion.[23,27] The stability criterion is generally accepted to be $\sigma \approx 0.02$,[23,27] and we assume that that the tip diameter is roughly equal to the wire diameter ($2\rho' \approx 2\rho$). We plot v_{tip} versus ρ on a log−log plot in the inset of Figure 4, and as expected from eq 2, at high values of ρ we find a slope of −2, stemming from the ρ^{-2} dependence. From this fit, assuming d_0 is on the order of 10^{-7} cm,[24] we find that the diffusion coefficient of H_2PtCl_6 in aqueous solution is on the order of $D = 10^{-8}$ cm^2/s. This diffusivity is consistent with other measures of Pt precursor diffusion, as the diffusion coefficient of K_2PtCl_4 in an ionic solution has been reported to be $D_{ionic} = 10^{-7}$ cm^2/s.[28] The good qualitative fit to eq 2 suggests that the simple diffusion model is a valid first order approximation to describing DENA, however, this simple calculation does not include effects of electromigration or electroconvection that can play a role in these electrochemical systems.[29]

dx.doi.org/10.1021/nl1039956 |Nano Lett. XXXX, XXX, 000–000

At low values of ρ, the plot does not follow the linear log−log fit; however, the shape of the plot is consistent with experiments on classic dendritic growth by Glicksman.[27]

The frequency also controls the morphology of growth through the growth rate dependence. As shown in the top scanning electron microscopy (SEM) panels of Figure 4, increasing the frequency causes the morphology to change from faceted needlelike dendrites to dendrites with bumpy surfaces in which many nucleation sites are observed. These protuberances arise because the rapid growth velocity at high ω, as newly reduced Pt adatoms do not have time to diffuse away from the tip.

We also find that an ac potential, as opposed to dc, is necessary for dendrite growth. Under a constant dc potential, increasing the magnitude beyond roughly 1.5 V_{dc} causes bubbles of H_2 and O_2 to form violently in solution due to electrolysis. This agitation mechanically disrupts wire growth and prevents stable nanowires.

Thus single, high aspect ratio nanowires may be grown via the combination of low voltage magnitude, addition of NaCl, and high ac frequency. A typical nanowire is shown in Figure 5 and features a high aspect ratio of 60 μm × 100 nm, minimal side branching, and most importantly bridges the gap between the two microelectrodes. Growth conditions for this wire are a 24 mM chloroplatinic acid solution with 89 mM NaCl, an applied potential of 16 V_{pp} at 8 MHz, V_0 = 0, and 50% duty cycle.

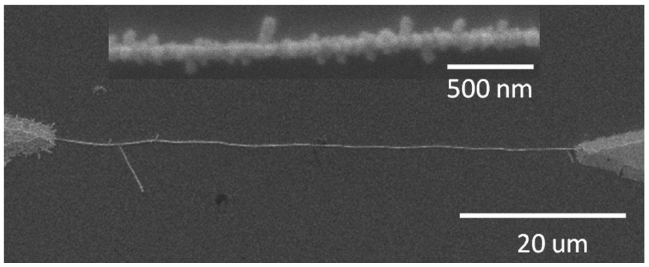

Figure 5. SEM of a single Pt nanowire, 60 μm × 100 nm, that bridges the gap between the electrodes. This nanowire was grown from a 24 mM chloroplatinic acid solution with 89 mM NaCl, an applied potential of 16 V_{pp} at 8 MHz, V_0 = 0, and 50% duty cycle.

Figure 6 shows time lapse images of typical DENA growth taken in situ under an optical microscope with no dc offset and a 50% duty cycle. We find that the mechanism of directed growth is a combination of anisotropic diffusion and dielectrophoresis (DEP). Panels a−c of Figure 6 show the onset of dendrite growth. Here we see that both the main stem and the side-branches preferentially grow faster toward the pulsed electrode (right side of image) as compared to the perpendicular direction. The likely cause for this faster growth is the spatially dependent intensity of the electric field. From the electrode geometry, one can show that the electric field is higher in the regions between the electrodes than in the regions away from the electrodes. This high field leads to a high Pt ion concentration in the electrode gap and thus faster growth in the gap than away from the gap.

Examination of panels d−f in Figure 6 reveals evidence of the physical bending process. After the wires grow beyond a certain threshold length, they begin to bend toward the opposing pulsed electrode. This bending is caused by dielectrophoretic (DEP) in which a nonuniform electric field induces a dipole moment on a neutral particle in solution, and the resulting moment acts to align the particle with the field.[30] This DEP force has been shown to align pregrown nanowires and nanoparticles in solution,[8,9,15] and in this case a similar effect occurs on growing nanowires.

But not only does the driving force set the direction of growth, it also sets the initial site of nucleation. We find that the sign of the dc offset sets the site of nucleation. Figure 7 shows that with a dc offset of $V_0 \geq 0$, growth typically begins on the grounded electrode and proceeds toward the pulsed electrode, while with a dc offset of $V_0 < 0$, growth typically proceeds in the opposite direction, from the pulsed electrode toward the ground. In general, growth initiates on the electrode that is more negatively biased. Changing the duty cycle has a similar effect as changing the dc offset in that a duty cycle ≥50% (net positive dc offset) leads to growth beginning on the grounded electrode, and a duty cycle <50% (net negative dc offset) leads to growth on the pulsed electrode.

We have demonstrated the synthesis and control of nanoscale dendrites and wires using the DENA method. This approach enables the scalable and rapid growth of Pt nanostructures at

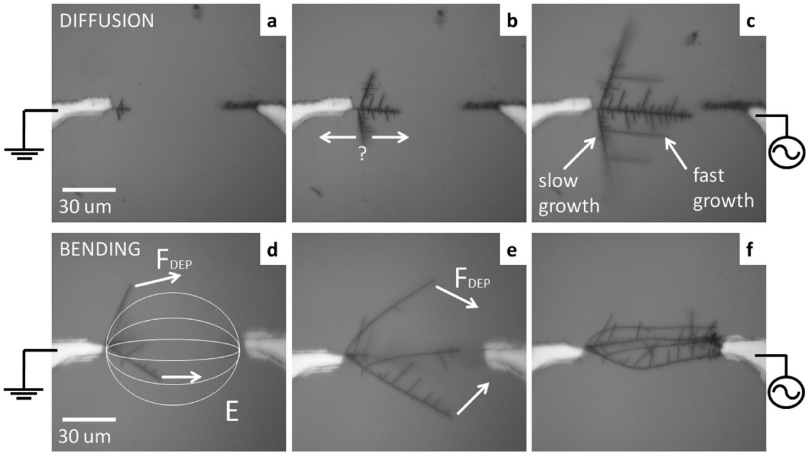

Figure 6. Two mechanisms for directed growth, shown in time lapse images from left to right taken under an optical microscope. (a−c) Anisotropic diffusion growth (12 V_{pp} at 2 MHz). Side branches emanating from the vertical dendrites grow faster toward the right (toward the electrode gap) than toward the left (away from the electrode gap). (d−f) DEP bending (12 V_{pp} at 4 MHz). Dielectrophoresis aligns the nanowires with the electric field, thus bending the growing nanowires toward the opposing electrode. The DEP force is more noticeable on the bottom panels than on the top panels because the thinner wires on the bottom (200 nm diameter) are more easily bent than the thicker wires on the top (700 nm diameter).

dx.doi.org/10.1021/nl1039956 |*Nano Lett.* XXXX, XXX, 000–000

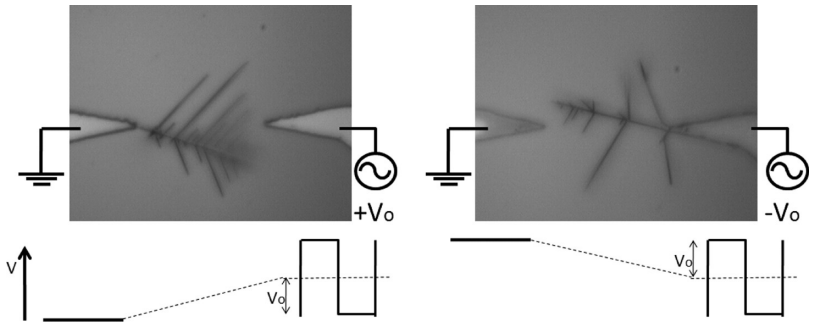

Figure 7. Pt DENA growth for positive (left) and negative (right) dc offsets. The dc offset sets the side of dendrite nucleation, as dendrite growth occurs at the site of lower overall potential.

predefined locations. By mapping the experiment onto classical dendrite growth theory, we explain the dependence of observed morphology on the growth parameters. In contrast to the classical examples of dendrite growth, where the tip velocity, tip radius, and degree of side branching are all controlled by the magnitude of a dc driving force, we find that in DENA these dependencies are decoupled allowing greater control over the structures obtained. Here the degree of sidebranching is primarily controlled by the magnitude of the applied potential V_{pp}, whereas the tip diameter and velocity are controlled by the frequency ω. Moreover the addition of salt to the electroplating solution further reduces the degree of sidebranching. We have shown that careful control of driving parameters and salt addition enables the production of a variety of edge-supported nanostructures ranging from highly branched treelike dendrites to unbranched nanowires with high aspect ratio ($60\,\mu m \times 100$ nm). The nanostructures and synthesis method appear promising for a wide variety of applications such as sensors or catalysis in which the directed assembly of high aspect ratio or high surface area Pt materials are needed.

AUTHOR INFORMATION

Corresponding Author

*E-mail: cbarnold@princeton.edu.

Present Addresses

[†]Department of Materials, University of California, Santa Barbara.

ACKNOWLEDGMENT

The authors thank Nan Yao, Mikko Haataja, and Alexander Smits for useful discussions. Funding for this work was provided by the NSF (Grant CTS-0625268) and the Princeton Department of Mechanical and Aerospace Engineering John Marshall II Thesis Fund. Additionally, we acknowledge the usage of PRISM Imaging and Analysis Center that is supported in part by the NSF MRSEC program through the Princeton Center for Complex Materials (Grant DMR-0819860).

REFERENCES

(1) Wang, W.; Jia, F.; Huang, Q.; Zhang, J. *Microelect. Eng.* **2005**, *77*, 223–229.
(2) Bailey, S. C. C.; Kunkel, G. J.; Hultmark, M.; Vallikivi, M.; Hill, J. P.; Meyer, K. A.; Tsay, C.; Arnold, C. B.; Smits, A. J. *J. Fluid Mech.* **2010**, *663*, 160–179.
(3) Shui, J.; Li, J. *Nano Lett.* **2009**, *9*, 1307–1314.
(4) Martin, C. R. *Science* **1994**, *266*, 1961–1966.
(5) Yi, G.; Schwarzacher, W. *Appl. Phys. Lett.* **1999**, *74*, 1746–1748.
(6) Li, Q.; Koo, S.; Richter, C.; Edelstein, M.; Bonevich, J.; Kopanski, J.; Suehle, J.; Vogel, E. *IEEE Trans. Nanotechnol.* **2007**, *6*, 256–262.
(7) Pauzauskie, P.; Radenovic, A.; Trepagnier, E.; Shroff, H.; Yang, P.; Liphardt, J. *Nat. Mater.* **2006**, *5*, 97–101.
(8) Smith, P.; Nordquist, C.; Jackson, T.; Mayer, T.; Martin, B.; Mbindyo, J.; Mallouk, T. *Appl. Phys. Lett.* **2000**, *77*, 1399–1401.
(9) Liu, Y.; Chung, J.; Liu, W.; Ruoff, R. *J. Phys. Chem. B.* **2006**, *110*, 14098–14106.
(10) Lee, S.; Lee, H.; Oh, D.; Lee, S.; Goto, H.; Buckmaster, R.; Yasukawa, T.; Matsue, T.; Hong, S.; Ko, H.; Cho, M.; Yao, T. *J. Phys. Chem. B* **2006**, *110*, 3856–3859.
(11) Decker, C.; Solanki, R.; Freeouf, J.; Carruthers, J.; Evans, D. *Appl. Phys. Lett.* **2004**, *84*, 1389–1391.
(12) Yun, M.; Myung, N. V.; Vasquez, R. P.; Lee, C.; Menke, E.; Penner, R. M. *Nano Lett.* **2004**, *4*, 419–422.
(13) Sanles-Sobrido, M.; Correa-Duarte, M.; Carregal-Romero, S.; Alvarez-Puebla, B.-G. R.; Herves, P.; Liz-Marzan, L. *Chem. Mater.* **2009**, *21*, 1531–1535.
(14) Rashid, M.; Mandal, T. *J. Phys. Chem. C* **2007**, *111*, 16750–16760.
(15) Hermanson, K.; lumsdon, S.; Williams, J.; Kaler, E.; Velev, O. *Science* **2001**, *294*, 1082–1086.
(16) Wen, X.; Xie, Y.; Mak, M.; Cheung, K.; Li, X.; Renneberg, R.; Yang, S. *Langmuir* **2006**, *22*, 4836–4842.
(17) Teng, X.; Yang, H. *Nano Lett.* **2005**, *5*, 885–891.
(18) Ozturk, B.; Flanders; Grischkowsky, D.; Mishima, T. *Nanotechnology* **2007**, *18*, 1–8.
(19) Cheng, C.; Gonela, R.; Gu, Q.; Haynie, D. *Nano Lett.* **2005**, *5*, 175–178.
(20) Talukdar, I.; Ozturk, B.; Flanders, B.; Mishima, T. *Appl. Phys. Lett.* **2006**, *88*, 1–3.
(21) Ozturk, B.; Talukdar, I.; Flanders, B. *Nanotechnology* **2007**, *18*, 1–10.
(22) Harris, P. *Surf. Sci. Lett.* **1987**, *185*, L459–L466.
(23) Langer, J. S. *Rev. Mod. Phys.* **1980**, *52*, 1–28.
(24) Glicksman, M. E.; Lupulescu, A. O. *J. Cryst. Growth* **2004**, *264*, 541–549.
(25) Barton, J. L.; Bockris, J. O. *Proc. R. Soc. London, Ser. A* **1962**, *268*, 485–505.
(26) Wagner, F.; Moylan, T. *Surf. Sci.* **1989**, *216*, 361–385.
(27) Huang, S.; Glicksman, M. *Acta Met.* **1981**, *29*, 701–715.
(28) He, P.; Liu, H.; Li, Z.; Li, J. *J. Electrochem. Soc.* **2005**, *152*, 146–153.
(29) Wang, M.; Zhong, S.; Yin, X.-B.; Zhu, J.-M.; Peng, R.-W.; Wang, Y.; Zhang, K.-Q.; Ming, N.-B. *Phys. Rev. Lett.* **2001**, *86*, 3827–3830.
(30) Pohl, H. *Dielectrophoresis*; Cambridge University Press: New York, 1978.

dx.doi.org/10.1021/nl1039956 |*Nano Lett.* XXXX, XXX, 000–000